Distributed Temperature Alarm System Based on Incoherent Optical Time-Domain Reflectometry and Side Air-Hole Optical Fibers

Yuting Yang, Marcelo A. Soto, *Member, IEEE*, and Luc Thévenaz, *Fellow, IEEE*

***Abstract*— This paper proposes and experimentally validates a distributed temperature alarm system based on carbon dioxide (CO_2)-filled 18 m side air-holes fiber (SAHF), interrogated through a conventional (incoherent) optical time-domain reflectometer (OTDR). Customizable alarm threshold temperatures can be designed and set by adjusting the pressure of the CO_2 filling the air-hole region, which in turn determines a threshold temperature under which CO_2 liquefies. The observed slopes of the backscattered Rayleigh intensity trace as a function of the position along the fiber serve as indicators of the CO_2 states, allowing the identification of both gaseous and liquid phases through variations in the optical attenuation. Utilizing a comparative analysis of curve slopes, the proposed method enables the distributed identification and localization for both cold and hot spots along the fiber. The spatial resolution and the required loss accuracy are subject to the classical tradeoff inherent to OTDR interrogation. In this study, two interrogation wavelengths (namely, 1310 nm and 1550 nm) are exploited. Results point out that the selection of the operating wavelength gives rise to optical attenuation factors with distinct contrasts along the OTDR traces, allowing the optimization of the system to meet specific measurement objectives. In particular, the use of an optical source at 1550 nm demonstrates superior measurement accuracy within short fiber lengths, revealing a higher loss contrast between gas and liquid phases. Conversely, a 1310 nm light source is deemed more suitable for long-distance monitoring due to the lower optical loss in cold spots (CO_2 in liquid phase), providing relevant measurements over extended cooled fiber sections. Based on our experimental results using a spatial resolution of 30 cm, the maximum detection length is limited to 36.0 m or 16.0 m at 1310 nm or 1550 nm, respectively, which take place when all CO_2 liquefies inside the fiber.**

***Index Terms*— Distributed sensing, fiber optics, optical fiber sensors, optical time-domain reflectometry, temperature sensors.**

I. Introduction

In various monitoring scenarios and applications, there exist a need to identify specific locations where the temperature exceeds or falls below a predefined critical threshold value. This could involve natural environment monitoring (e.g. icing of land and lakes, or spring landslides caused by ice melting), public utilities monitoring (e.g. overheating along power cables, or ice formation along roads) and hazard monitoring (e.g. detecting leaks in heating pipelines or liquefied natural gas), among other situations. In many cases, the use of a fully distributed temperature sensor, such as a fiber-optic Raman, Brillouin, or Rayleigh distributed sensors [1] may be overqualified, too complex and too expensive for this purpose. Therefore, the use of simpler and cost-effective solutions would be preferable.

In this context, this paper proposes a comprehensive distributed temperature alarm system based on a gas-filled side air-holes fiber (SAHF), which is interrogated by a simple and cost-effective conventional (incoherent) optical time-domain reflectometer (OTDR). The method relies on the substantial alteration in optical loss caused by a gas undergoing a phase transition from vapor to liquid at a specific temperature [2]. Through this approach, the proposed system binarily identifies and localizes sections along the fiber where the temperature surpasses or falls below a predefined threshold value, as previously sketched in a rudimentary non-distributed configuration [3]. To achieve this objective, the small evanescent field present in the SAHF proves adequate for detecting alterations in the optical loss when the gas in the air holes undergoes liquefaction [4]. This is performed by introducing carbon dioxide (CO_2) into the air holes at a specific pressure, which must be carefully selected to facilitate the gas liquefaction below the designated temperature threshold. The pressure conditions are selected to secure the vapor-to-liquid phase transition at a targeted temperature threshold. Experimental results validate the capability of the method to provide distributed monitoring of the gas phase transitions along the fiber, thereby enabling the implementation of a distributed temperature alarm system.

Manuscript received January 27, 2024. This research was supported in part by the projects C21-13 of the Swiss Data Science Centre and Innosuisse 38390.1. M. A. Soto thanks the support of Chilean National Agency for Research and Development (Fondecyt Regular 1241085 and Basal FB0008).

Y. Yang and L. Thévenaz are with the Institute of Electrical Engineering, Swiss Federal Institute of Technology of Lausanne (EPFL), CH 1015 Lausanne, Switzerland (e-mail: yuting.yang@epfl.ch, luc.thevenaz@epfl.ch).

Marcelo A. Soto is with the Department of Electronic Engineering, Universidad Técnica Federico Santa María, 2390123 Valparaíso, Chile (e-mail: marcelo.sotoh@usm.cl).

Color versions of one or more of the figures in this article are available online at http://ieeexplore.ieee.org

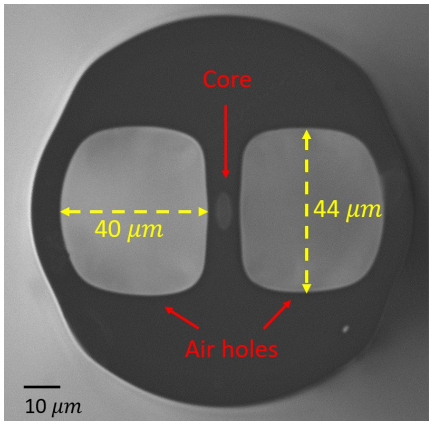

Fig. 1. SEM picture of the side air-holes fiber (SAHF) cross-section.

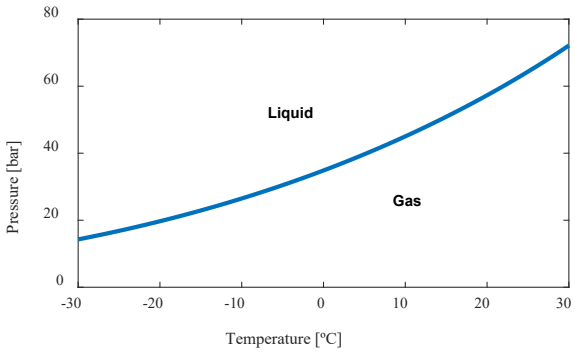

Fig. 2. CO_2 vapor-to-liquid phase transition diagram, from -30ºC to 30ºC.

II. Principle

The principle of the proposed method is based on the changes in the optical field distribution and optical loss experienced by the light propagating in a SAHF under different gas phase states. In this work, the holes of the fiber shown in Fig. 1 are filled with carbon dioxide, undergoing a transition from a gaseous to a liquid phase when the ambient temperature falls below a specified critical threshold. This threshold temperature highly depends on the gas pressure inside the fiber. Consequently, in order to devise an alarm system responding to a specific critical temperature, it is relevant to meticulously determine the appropriate pressure required to inject the gas inside the fiber.

For CO_2, the semi-empirical relationship between the pressure (P) and temperature (T) along the coexistence curve in the phase diagram can be written as [5]:

$$\ln\left(\frac{P}{p_c}\right) = \frac{T_c}{T}\cdot\left[\sum_{i=1}^{4} a_i\left(1-\frac{T}{T_c}\right)^{t_i}\right]. \quad (1)$$

with p_c and T_c denoting the critical point of CO_2, marking the pressure and temperature at which the distinction between liquid and gas can no longer be made: p_c=7.3773 MPa for T_c=304.1282 K. The coefficients t_i and a_i (with $i = 1, 2, 3, 4$) are empirical coefficients determined through fitting to vapor pressure measurements: t_1 =1.0, t_2 =1.5, t_3 =2.0, t_4 =4.0, a_1 =-7.0602087, a_2 =1.9391218, a_3 =-1.6463597, a_4 =-3.2995634 [5]. In this case, the vapor-to-liquid phase transition can be predicted based on (1).

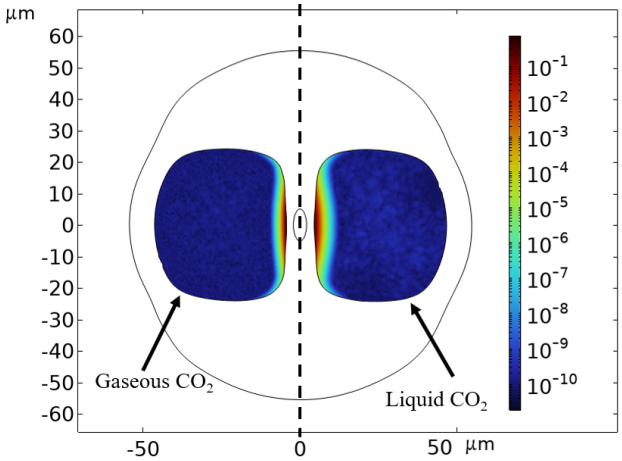

Fig. 3. Simulation results of the normalized evanescent field distribution for gaseous (left hole) and liquid CO_2 (right hole) in a synoptic view for best comparison. To compare the ratio of the field merged into the side air-holes, the calculated field is normalized with the maximum field in the core.

Fig. 2 shows the pressure of the CO_2 inside the air-holes of the fiber required to trigger the vapor-to-liquid phase transition as a function of the temperature in ambient conditions. This figure serves as a guide for determining the required pressure of the CO_2 inside the air-holes of the fiber to attain a target temperature threshold. The behavior shows that high phase-transition temperatures (i.e. for alerts at high temperatures) can be achieved by very high gas pressures (e.g. for the transition to occur at a room temperature of 20ºC, a pressure of 57.3 bar is needed); while the reduction of the critical temperatures implies the use of lower pressures (still higher than atmospheric pressure) to fill the CO_2 inside the SAHF. For instance, defining a target threshold temperature of 2.3ºC to trigger the alarm of the proposed sensor, a pressure of 37 bar is required for the CO_2 introduced into the air-holes of the fiber.

During the transition from vapor to liquid phase, the optical properties within the air-holes change according to the state of the medium. Fig. 3 shows the transversal distribution of the optical field within the side holes of the fiber, simulated using COMSOL (using a cladding refractive index=1.44, and a core refractive index=1.455), when the SAHF is filled with gaseous and liquefied CO_2. The fiber structure contouring for the simulation is obtained from the SEM picture (Fig. 1) of the SAHF cross section. Subsequently, the optical field is calculated separately, with different refractive indices for gaseous and liquefied CO_2.

It must be noted that, the refractive index n for liquefied CO_2 is not readily available in the literature and can be estimated according to the Clausius-Mossotti relation [6]:

$$\frac{n^2-1}{n^2+2} = \frac{N_A\rho\alpha}{3M}. \quad (2)$$

where N_A refers to the Avogadro's constant; ρ is the density of CO_2 which is 1.77 kg/m^3 at 26.85°C under 1 bar for gaseous CO_2 and 1117 kg/m^3 at -40°C under 10 bar for liquefied CO_2 [7]; $M = 44\times10^{-3}\ kg/mol$ is the molar mass of CO_2; α represents the polarizability of CO_2 molecules, which remains constant regardless of the state – gas or liquid. When applying the equation to describe gaseous CO_2, the sole unknown value

is the polarizability α, which can be derived from the known refractive index and density (n =1.0004 under 1 bar [7]). Regarding the low compressibility of liquids, we assume that the density of liquefied CO_2 is independent of pressure. Utilizing the obtained value of α from the prior step and the constant density for liquefied CO_2, resolving (2) allows us to estimate the refractive index for liquefied CO_2 as n=1.2677.

During the liquefication of the CO_2, the phase transition occurs over a temperature change of less than 1°C or a pressure difference of less than 1 bar, nominally at constant temperature and pressure. In this prospect, all the effects in the fiber due to thermal and pressure expansions are totally negligible. Indeed, the thermal effects are orders of magnitude smaller than the massive change of the CO_2 refractive index ($\Delta n = 0.2673$) when passing from gas to liquid.

Actually, and being a bit counterintuitively, our simulations show that the difference between the $1/e$ penetration depths of the evanescent fields in the gaseous ($0.10\ \mu m$) or liquefied CO_2 ($0.13\ \mu m$) scenarios is not that large, since the decay of the electrical field follows a similar distribution in both cases. The essential difference is due to the step transition of the permittivity between silica and holes, which scales the amplitude of the electric field at the interface between silica and holes. The key parameter here describing penetration is the fraction of electric flux in the side air-holes region, defined as the surface integral of the electric field in the holes. According to the COMSOL simulation, for the gaseous CO_2 scenario, the optical power (obtained as proportional to the simulated electric flux squared) in the two side holes is 0.00098% of the total power, while the effective refractive index is 1.4550. For the liquefied CO_2 scenario, the optical power in the two side holes is 0.0037% of the total power, while the effective refractive index is 1.4551.

In the scenario of liquefied CO_2, the penetration of the optical field into the side-holes area is approximately 4 times larger compared to that observed with gaseous CO_2. However, these numbers show that only ~0.001% of the total power is present in the holes, highlighting the fact that the differential absorption between gas and liquid is more relevant than the difference in penetration.

Similar to its gaseous state, liquid CO_2 exhibits an absorption band centered at 1572 nm, but much broader and widely covering the conventional wavelengths of 1550 nm and 1310 nm. This absorption band indeed extends well beyond the absorption band of gaseous CO_2 [8], which shows reduced absorption at those wavelengths. Consequently, the transition from gaseous CO_2 to liquid CO_2 results in a higher presence of light propagating through a medium characterized by increased optical absorption, leading to significantly higher optical attenuation. As a result, when the temperature at specific positions along the SAHF falls below the predetermined threshold, gaseous CO_2 locally liquefies causing fiber sections with higher losses, which can be identified using a conventional OTDR instrument.

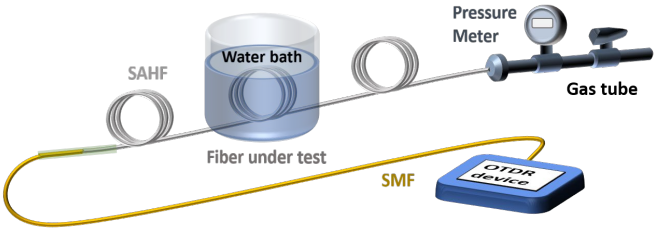

Fig. 4. Experimental validation setup. An OTDR instrument is used to interrogate a CO_2-filled SAHF. The OTDR is connected through a standard single-mode fiber spliced to the SAHF. The far end of the SAHF is connected to a tube filled with CO_2 at specific gas pressures. A water bath is employed to control the temperature of some sections of the optical fiber under test.

III. Experimental Demonstration

To demonstrate the feasibility of the proposal, the experimental implementation is rooted on a very basic classical scheme based on optical time-domain reflectometry.

A. Experimental Setup

Fig. 4 shows the experimental setup used to validate the proposed method, in which an incoherent OTDR instrument is employed for interrogation. An 18 m-long SAHF serves as a medium to confine the CO_2 in the side air-holes, while guiding incoherent light in the core region. One end of the SAHF is spliced to a standard single-mode fiber in order to establish a fine connection with the OTDR device. The effective dynamic range of the OTDR trace is 15 dB, which is given by the instrumental dynamic range, and reduced by the coupling loss between SMF and SAHF. Simultaneously, the other end of the SAHF is connected to a gas supply via a gas tube equipped with a precision manometer. This configuration allows for monitoring the injection of gaseous CO_2 at different pressures while neglecting potential transient pressure gradients along the system. Both fiber ends are kept gastight; however, in a practical sensor application, the far end of the SAHF connected to the gas tube must also be sealed after filling the fiber at the target pressure. For instance, this can be performed by splicing the end with a standard solid core fiber or collapsing the fiber holes at the free end, so that the fiber is turned into a hermetic silica rod. The system is pre-vacuumed to eliminate the influence of air, ensuring that the residual air is left below 10 mbar. This has certainly a negligible impact when considering a working CO_2 pressure during the measurement three orders of magnitude higher.

The initial measurements use a light source at 1550 nm, achieving the finest spatial resolution of approximately 30 cm in silica by using 3 ns incoherent light pulses. The built-in photoreceiver of the OTDR interrogator captures the Rayleigh backscattered signal along the fiber, with an equivalent spatial sampling of 5 cm. To enhance the visualization of the measured OTDR traces, a smoothing low-pass filter is applied over a spatial window of 6 neighboring points in order to benefit from the oversampling spanning the spatial resolution.

To change the temperature of distinct fiber sections with high precision, sections of the SAHF are immersed into a water bath, ensuring a thermal accuracy of about 1°C while changing the temperature over a wide range.

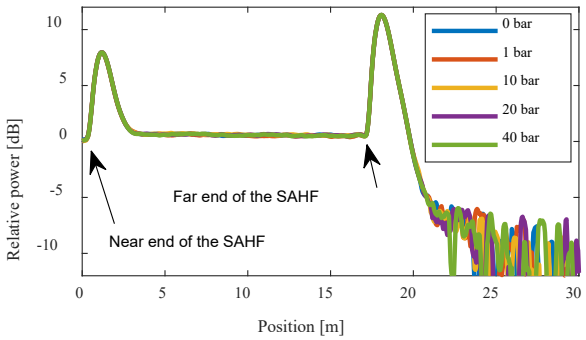

Fig. 5. Room temperature measurements of the SAHF backscattering signal at different CO_2 pressures, while ensuring the gaseous state of CO_2. No significant induced losses are evident in the measurements.

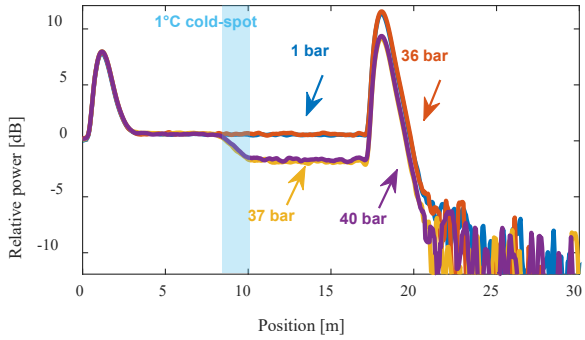

Fig. 6. Measurements of the SAHF backscattering signal at different pressures from 1 bar to 40 bar. The light blue shading indicates the optical fiber segment placed at a constant temperature of 1°C. An additional optical loss appears in the cold region when the CO_2 pressure is increased up to 37 bar or higher.

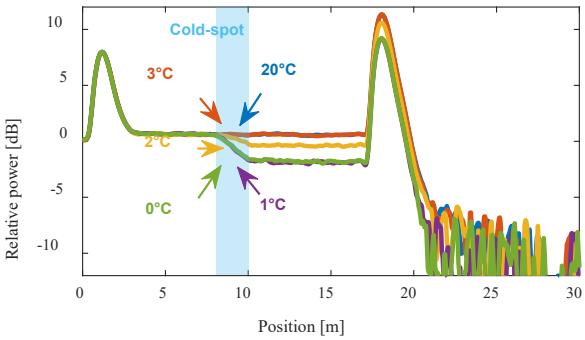

Fig. 7. Measurements of the SAHF backscattering signal at a constant pressure of 37 bar. A fiber section, marked by the light blue shading, is cooled from room temperature (20°C) down to 0°C. Induced losses are clearly observable for all temperatures below 3°C and remain steady below 1°C.

B. Impact of Pressure Changes

The initial measurements are conducted to assess the optical loss of the SAHF under different internal pressures of the gaseous CO_2. The test is performed using a broadband light source centered at 1550 nm, while maintaining the entire fiber at room temperature. Fig. 5 shows the OTDR traces obtained for different CO_2 pressures, ranging from 0 bar to 40 bar, over which CO_2 keeps in a gaseous state at room temperature. Results show that all OTDR traces are the same under the different pressures, confirming no significant induced loss and no impact of the CO_2 pressure. This validates the combined effect of negligible gas molecular absorption and of a minor fraction of the evanescent field present in the air holes, while filled with gaseous CO_2. This also emphasizes the robust structure of the air holes, ensuring undistorted waveguiding conditions along the propagation path even under an internal pressure of 40 bar.

To evaluate the impact of CO_2 liquefication in the side air holes, a section of the fiber (position from 8 m to 10 m) is cooled down to 1°C while other sections are maintained at room temperature (about 20°C). Referring to the CO_2 phase diagram in Fig. 2, the phase transition from gaseous CO_2 to liquid CO_2 at a temperature 1°C takes place at a CO_2 pressure of about 35.8 bar, while the required temperature for liquefication is 57.3 bar at the room temperature of 20°C.

Measurements are performed while varying the pressure of the CO_2 filled in the side air-hole from 1 bar to 40 bar. According to Fig. 2, CO_2 keeps gaseous throughout the experiment in the fiber sections at room temperature since the pressure does not exceed 57.3 bar. However, in the fiber section cooled at 1°C, CO_2 undergoes a phase transition from gas to liquid as the pressure increases, when crossing the phase transition curve. Fig. 6 shows the OTDR traces obtained under the different tested pressures. To secure reliable results, each measurement is obtained after stabilizing the pressure for about half an hour. Results point out that when the pressure increases from 36 bar to 37 bar, the CO_2 undergoes a phase transition, leading to an additional optical loss between 8 m and 10 m. This can be observed by the steeper slope of the OTDR traces in the cooled fiber section, which is attributed to the formation of liquid CO_2, and not to any pressure change during the phase transition, as validated previously in Fig. 5.

According to the theoretical prediction in Fig. 2, the phase transition pressure at 1°C occurs at 35.8 bar; however, the measurements indicate a critical pressure between 36 bar and 37 bar. This slight discrepancy may arise from the inhomogeneities in the experimental setup, considering that the CO_2 gas pressure is measured from the pressure meter on the gas tube connected to the opened end of the SAHF. On the other hand, the temperature is measured inside the water bath, where the temperature may not be perfectly uniform.

C. Impact of Temperature Changes

As discussed in Section II, the phase transition point is subject to both temperature and pressure changes. In this section, the impact of temperature changes is analyzed while keeping a constant CO_2 pressure. Similar to pressure changes, any temperature variation will impact the phase transition, resulting in similar high loss signal in the cooled section of the OTDR traces.

For this test, the pressure of CO_2 filled in the side air-holes is kept constant at 37 bar. According to Fig. 2, at this pressure the phase transition temperature is about 2.3°C. In the experiment, a section of the fiber (position from 8 m to 10 m) is cooled to

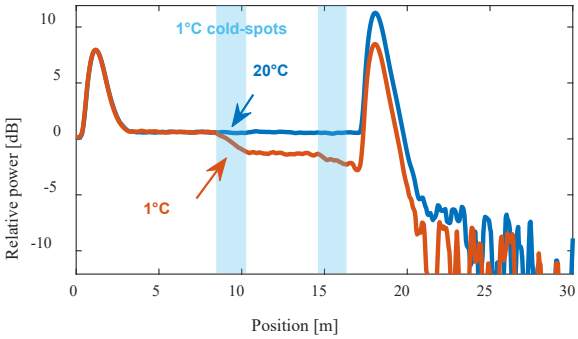

Fig. 8. Measurements of the SAHF backscattering signal at a constant pressure of 37 bar, incorporating distinct multiple cooled sections in the system. Two fiber sections, identified by the light blue shadings, are cooled from room temperature (20ºC) to 1°C. The successive induced losses along the two sections validates the potential for distributed sensing of multiple events along the fiber.

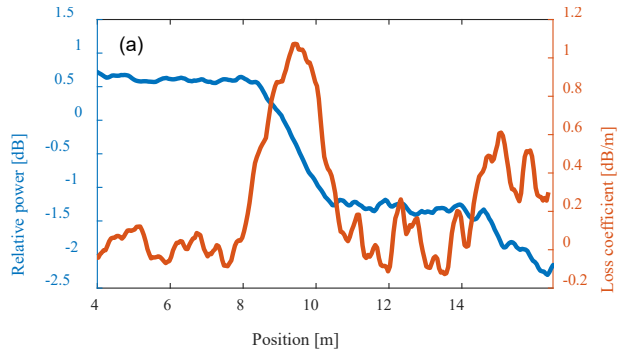

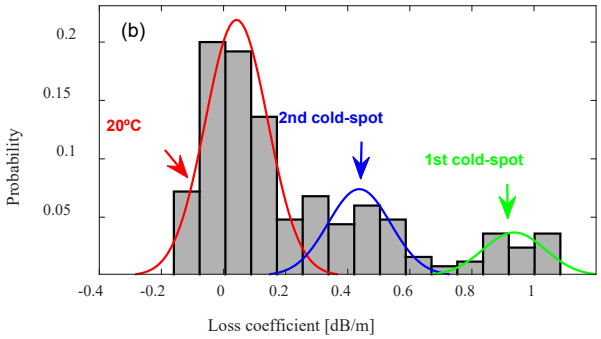

Fig. 9. Estimation of loss coefficients when measuring multiple cooled sections with a 1550 nm laser source. (a) OTDR trace (blue line) and estimated local loss (red line) based on the slope of OTDR traces. (b) Probability distribution of the estimated losses, obtained by a 3-Gaussian curve fitting, which is used to estimate the mean loss coefficient for the two cold spots (blue and green curves) and room temperature (20ºC, red curve).

different temperatures from room temperature (20ºC) down to 0°C, crossing the phase transition point. Similar to the pressure change process, under circumstances where the cooled section is above the critical temperature, CO_2 keeps gaseous, leading to a relatively flat OTDR trace all along the fiber, as shown by the blue and red curves in Fig. 7. When the cooled section is precisely at the critical temperature (measured at 2°C, slightly mismatched with the theoretical 2.3°C), CO_2 in the side air-holes exists as a mixture of gaseous and liquid states, showing partially higher loss, as depicted by the yellow line in Fig. 7. As the temperature of the cooled section continues to decrease, CO_2 completely liquefies, resulting in a consistent and stabilized high loss section, as shown by the violet and green curves in Fig. 7.

D. Distributed Multi Cold-Spot Measurements

Due to the spatially resolved information provided by the OTDR, the system also has potential for distributed sensing of multiple events, as the flow of gaseous CO_2 along the SAHF provides every point with an equal opportunity for liquefaction. To validate the distributed multi-event sensing capabilities of the system, measurements of multiple cold spots are carried out. For this purpose, two distinct fiber sections (from 8 m to 10 m and from 14 m to 16 m) are simultaneously cooled down to 1°C, while the rest of the fiber is maintained at room temperature, under a constant gas pressure of 37 bar. This condition enables CO_2 to liquefy in the cooled sections, while remaining in gaseous state within the fiber sections at room temperature. Fig. 8 shows the OTDR traces measured long the fiber. The additional loss coefficient induced by liquid CO_2 is evaluated by comparing it with the reference signal obtained from a uniformly gaseous CO_2 distribution (blue curve).

The determination of loss coefficients is based on the estimation of the local slope on the OTDR trace, which is computed using sampled points along the fiber within three spatial resolutions. The process assumes that the loss values in both room temperature and cold sections follow normal distributions, with the same standard deviation (this is based on the assumption of similar noise distribution and no systematic errors) and distinct mean values. Fig. 9(a) shows the OTDR trace around the cold spots (blue line) measured at 1550 nm and the estimated local loss based on the local slope calculation (red line). Note that the two cold spots show to have different local losses, which may be attributed to the inhomogeneous liquefaction of CO_2 inside the side air-holes due to a loss of uniformity in the gas pressure. This issue will be further discussed in the last section of the paper. To estimate the mean loss coefficients associated to the cold spots and room temperature, the probability distribution of the estimated losses is obtained, as shown in Fig. 9(b). This is carried out through a 3-Gaussian curve fitting, which allows us to estimate the mean loss coefficients associated to the two cold spots, shown by the blue and green Gaussian curves in the figure, and to the room temperature, shown by the red curve. Results indicate estimated loss coefficients of 0.94 dB/m for the first cold spot, 0.44 dB/m for the second cold spot, and 0.04 dB/m for the room temperature. It is worth mentioning that due to the short cold section of 2 m and restricted spatial resolution of 30 cm, only a few independent sampled points are available in this case, preventing us from performing a full, solid statistical analysis. This can be however improved in a future work, for instance using sharper spatial resolutions.

E. Impact of the Operating Wavelength

When conducting measurements with a 1550 nm light source, significant optical losses become evident in liquid CO_2

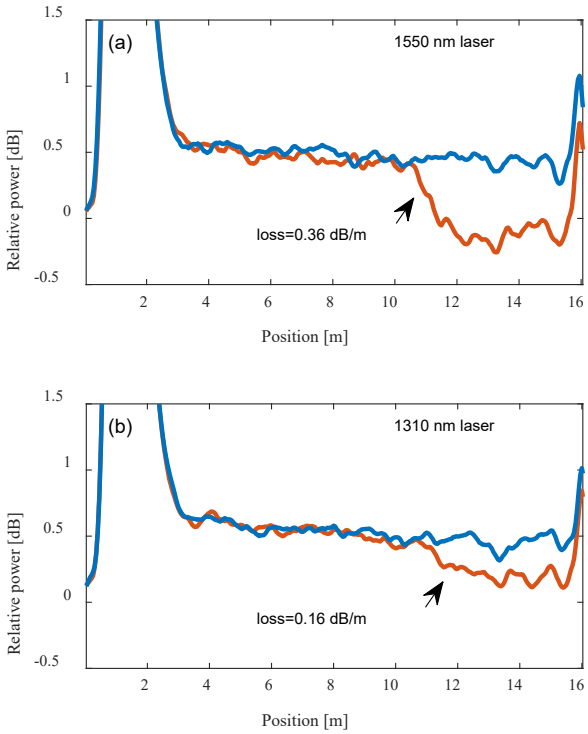

Fig. 10. OTDR traces measured with the entire fiber at room temperature (blue lines) and with a short fiber section (between 10.5 m and 12 m) placed at 1ºC (red lines), when using a laser source operating at (a) 1550 nm and (b) 1310 nm. The loss coefficient at 1550 nm in the cold fiber section is 2.25 times higher than that observed at 1310 nm.

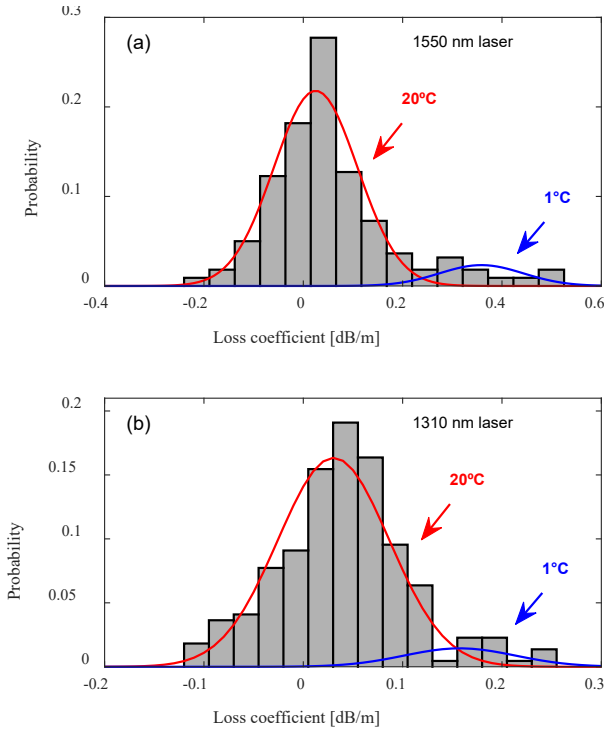

Fig. 11. Estimation of the optical loss coefficients based on a 2-peak Gaussian fitting of the probability distribution when using (a) a 1550 nm, and (b) a 1310 nm laser source. The red and blue curves indicate the fitting of the Gaussian distributions of loss coefficients at room temperature (20ºC) and cold fiber section.

sections. While the measurements exhibit good contrast, they face the challenge of rapid optical signal attenuation caused by the excessive loss, limiting the fiber length that can be interrogated. To extend distributed measurements over longer distances, a feasible approach is to vary the wavelength of the light source to be spectrally positioned away from the CO_2 absorption band at 1572 nm, thus securing a lower optical loss. Additionally, shorter wavelengths result in a better mode confinement in the core and thus in a more limited extension of the evanescent field into the side air holes (reduced by 57.3% according to our simulation), reducing even more the optical losses in liquid CO_2.

To evaluate the impact of the interrogating wavelength, measurements are carried out at both 1310 nm and 1550 nm. Fig. 10 shows the OTDR traces measured in the two cases, indicating that the optical losses reduce considerably in the liquid CO_2 regions, from 0.36 dB/m at 1550 nm down to 0.16 dB/m at 1310 nm. These values have been calculated following the same approach previously described based on the estimation of the local losses along the OTDR trace and a 2-peak Gaussian fitting, as depicted in Fig. 11 for both analyzed wavelengths. Note that this optical loss reduction represents a 2.25-fold difference between the two wavelengths, highlighting the flexibility to adapt the loss coefficient to the operating conditions and application, with an inherent tradeoff between sensing fiber length and loss coefficient accuracy.

The longest sensing distance that can be achieved by the proposed method can be estimated in the worst-case scenario, assuming that all the CO_2 in the side-holes is liquefied. In such a case, the propagation loss is maximized, limiting the maximum detection length to 16.0 m or 36.0 m when operating at 1550 nm or 1310 nm, respectively. This estimation is obtained dividing the 15 dB effective dynamic range of the OTDR measurements by the 0.94 dB/m loss coefficient, which represents the highest loss coefficient estimated across all measurements in the cold fiber sections. However, it is worth noting that these estimated maximum lengths can potentially be extended in practical scenarios where CO_2 liquefaction is incomplete or nonuniform along the fiber. In addition, it is possible to enhance the maximum detection length by extending (worsening) the spatial resolution or by increasing the response time through the use of extensive averaging, thus enabling a higher dynamic range of the OTDR traces. Alternatively, optimized fiber designs can be used to mitigate optical losses and extend the detection length. While in this first implementation the sensor is not yet capable of reaching kilometric distances, there is still space for improvement and optimization to extend the sensing distance.

F. Distributed Multi Hot-Spot Measurements

Considering that liquefication or evaporation can occur whenever the CO_2 temperature goes below or above the critical threshold temperature, the proposed method can also be exploited to measure hot spots. To verify this, the CO_2 pressure is set at 42 bar and the entire fiber is cooled down to 1ºC in the water bath. After stabilization, four short sections of the fiber

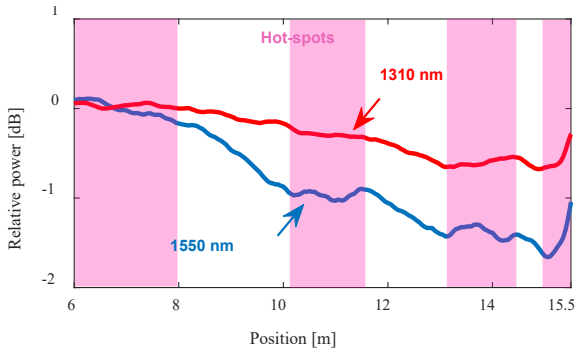

Fig. 12. Measurements of the SAHF backscattering signal at constant pressure of 37 bar in presence of distinct multiple hot spots (at room temperature), when the rest of the fiber is kept at 1ºC. Measurements are obtained at both 1550 nm (blue) and 1310 nm (red). The four fiber hot spots are indicated by the light red shading, by simply placing fiber segments out of the cold bath, so kept at a room temperature of 20ºC.

are moved out of water to increase their temperature up to room temperature. These four distinct fiber sections, designated as hot spots, remain separated by three cold sections at 1°C with varying lengths. Fig. 12 illustrates the distributed Rayleigh backscattered signal along the fiber, obtained at the two analyzed wavelengths. The light red shading area in the figure indicates the hot-spot sections, while the white areas correspond to the room temperature sections. As expected, the high loss coefficient obtained along the fiber at 1ºC is highly reduced in the hot fiber sections as a result of the CO_2 evaporation. Similar to the previous analysis, the use of an optical source at 1550 nm leads to a higher measurement contrast compared to the use of a source at 1310 nm, at the cost of reducing the maximum fiber length that can be interrogated.

To discern between cold and hot fiber sections, a threshold value can be established in the loss coefficient distribution using a statistical approach based on a confidence level of 50%. This ensures an equal likelihood, or 50% chance, for any given fiber section to be identified as cold or hot. Following this statistical approach and based on the probability distribution of the estimated loss coefficients, thresholds values of 0.21 dB/m and 0.099 dB/m are found for measurements with 1550 nm and 1310 nm, respectively. Fig. 13 shows the blind identification of hot fiber sections based on the OTDR measurements depicted in Fig. 12 for both operating wavelengths. Hot spots are depicted by light red shaded areas with dashed-line contours, showing a good matching with the actual hot sections in Fig. 12, especially for the case of using 1550 nm. However, a poorer identification is obtained when using 1310 nm, which could be improved as mentioned before, for instance, by compromising other OTDR parameters, such as the measurement time (to allow an enhanced dynamic range at the cost of a longer trace averaging process). It must be noted that, the threshold choice not only impacts the classification accuracy but also affects the uncertainty in localizing the hot and cold fiber sections, given our spatial resolution of 30 cm. Indeed, the determination of transitions is influenced by various factors, like the method to estimate the local slope of the OTDR trace, which may require a further investigation considering the observed statistical

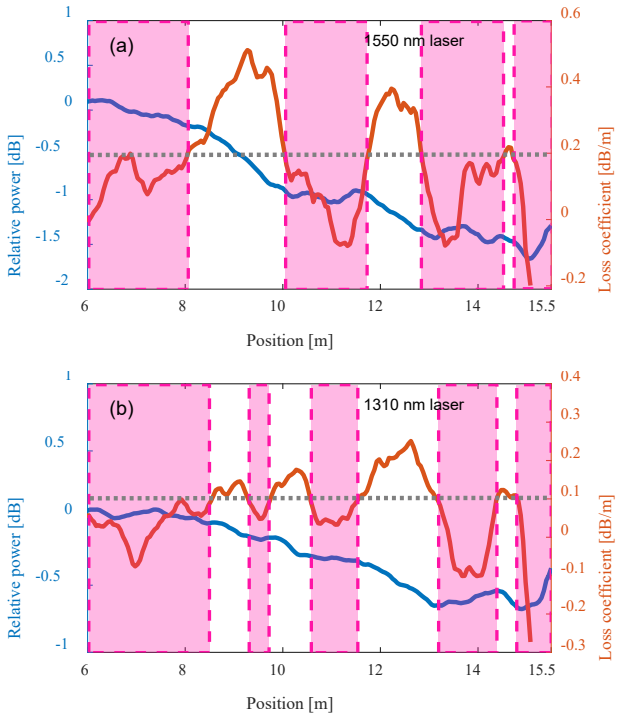

Fig. 13. Measured OTDR traces (blue lines) and estimated local loss coefficients (red lines) for (a) 1550 nm and (b) 1310 nm. The gray dotted lines show the blindly identified loss coefficient thresholds according to a 50% confidence level. Based on the proposed statistical approach, the light red shaded areas represent the fiber sections identified as hot spots.

variability. The carefully selection of the threshold value from the loss coefficient distribution is crucial to accurately classify regions as cold or hot spots, highlighting the critical importance of this aspect. The ability to measure hot spots proves valuable for monitoring potential issues such as hot water pipeline leaks or overheating along electrical power lines.

IV. Conclusions and Prospective Discussions

In conclusion, through the comparison of measurements conducted on a simple side air-holes fiber, we verified the feasibility of employing a CO_2-filled SAHF as a distributed temperature alarm system triggered by its vapor-to-liquid transition at a preset threshold temperature. The system can be effectively and simply interrogated using a standard OTDR instrument by analyzing the distributed profile of the optical losses along the fiber. Customization of the alarm temperature is achievable by filling CO_2 at a specific pressure in the air-hole region of the fiber. However, it is important to note that, for a given experimental setup, the spatial resolution of the measurements is highly dependent on the required accuracy in loss measurements, as ruled by the classical tradeoff affecting the OTDR measurement parameters.

The robustness of the system is verified by examining the impact of different CO_2 pressures on the fiber at room temperature, revealing negligible induced losses. This establishes a foundation for further exploration into the dynamic response of the fiber when filled with CO_2 and exposed to temperature variations.

The experiments conducted on the CO_2-filled fiber sections cooled below the threshold temperature under a constant pressure verified the influence of CO_2 phase transitions on the optical loss. The consistently low loss observed when the fiber temperature is above the critical temperature, and the subsequent rise in loss when the CO_2 transitions into a liquid state, provide clear evidence of the system's sensitivity to the physical state of the gas. The consistent reproducibility of the results, when varying either temperature or pressure, gives a high confidence in the high reliability of the system.

The adaptability of the system is demonstrated by varying the wavelength of the light source. For more accurate measurements, an optical source at 1550 nm is preferable because it shows a higher loss contrast between gas and liquid. However, for long-distance monitoring, a light source at 1310 nm is a better choice as it can provide relevant measurements over extended cooled fiber sections, owing to its lower loss per unit length as a result of the reduced optical absorption at this wavelength.

Relying on the same methodology, the scheme is also capable of measuring hot spots by reversing the approach used in the cooling experiments. By analyzing the slope of the OTDR trace, representing the local loss coefficient of the fiber, the boundary between gaseous and liquefied CO_2 states can be identified. This promising functionality extends the system's applications beyond cold spot measurements, such as monitoring frozen roads, to include hot spot measurements, like detecting potential damages to electrical lines.

However, it must be noted that the experimental attenuation coefficients are not completely consistent with the prediction: for instance, a different linear attenuation is observed in two distinct cold spots, though they are at the same temperature, as shown in Figs. 8 and 9. This behavior is likely attributed to an incomplete liquefaction of the CO_2 in certain cooled sections, logically leading to a lower attenuation, as illustrated in Fig. 7 when the temperature of the fiber section is in the close vicinity of the transition temperature. The difference in the response of two cold spots placed under similar environmental conditions can be explained by examining the gas dynamics within the fiber holes: in a hermetically sealed volume, the number of gas molecules is fixed and constant. If CO_2 is in a gaseous state along the entire fiber, the gas density and pressure remain uniform, resulting in an even response of the fiber to the presence of a cold spot at any position.

However, the liquid phase shows a significantly higher molecular density, resulting in a depletion of the molecule density in surrounding fiber sections where CO_2 remains in a gaseous state. Consequently, the gas pressure decreases around the cold spot, causing a shift in the threshold temperature to a higher level. The distance from the cold spot over which the effect of gas depletion is significant depends on the hole cross-section and time, scaling in a matter of seconds to span over 1 meter in the SAHF under test [9].

To circumvent this issue, several solutions can be foreseen. All of these solutions involve diluting the liquefying gas into a buffer gas that remains in a gaseous state across the entire operating temperature and pressure range (e.g. nitrogen over a very extended range around ambient temperature). The ideal case would be that the mixture turns into a cloud-like state when the diluted gas reaches its vapor saturation state and creates suspended droplets in the buffer gas. This would lead to a significantly enhanced light scattering, which would be best leveraged in hollow core fibers.

Unfortunately, cloud forming is subject to strict environmental conditions and results from the adiabatic cooling of a large mixed gas volume [10], like in the atmosphere when an air mass expands and cools down by natural convective up-motion, and then turns into a cloud from a given altitude when the diluted water vapor reaches saturation. These adiabatic conditions can never be realized in a fiber holey structure, since thermal exchange through the silica walls is overwhelmingly dominant regarding the microscopic size of the fiber structure.

The most probable situation is that the diluted gas condensates on the silica walls, creating a thin liquid film without significantly depleting the overall gas density away from the cooled section. Even though the observed change in attenuation would not be as strong as in the demonstrative case shown in this paper, there is enough room for optimization by shifting the interrogation wavelength closer to the center of the gas absorption band and in the design of the fiber microstructure. This shows that this novel class of fiber sensors, with considerable application potential, remains an attractive topic of research with plenty of room for smart designs and innovative solutions.

REFERENCES

[1] A. H. Hartog, *An Introduction to Distributed Optical Fibre Sensors* (1st ed.), CRC Press, 2017

[2] J. M. Yeomans, *Statistical mechanics of phase transitions*, Clarendon Press, 1992, pp. 1-3.

[3] L. Zhang, F. Yang, F. Gyger, and L. Thévenaz, "Distributed fiber temperature alarm system based on thermodynamic phase transition,". in *Optical Fiber Sensors*, 2020, pp. T2B-3.

[4] Y. Yang, M. A. Soto, and L. Thévenaz, L, "Distributed alarm system based on OTDR interrogation of side air-hole fibers", presented at the *28th International Conference on Optical Fiber Sensors* (OFS-28), Hamamatsu, Japan, Nov. 20-24, 2023.

[5] R. Span, and W. Wagner, "A new equation of state for carbon dioxide covering the fluid region from the triple‐point temperature to 1100 K at pressures up to 800 MPa," *Journal of physical and chemical reference data*, 25, no. 6, pp. 1509-1596, Nov. 1996.

[6] P.V. Rysselberghe, "Remarks concerning the Clausius-Mossotti law," *The Journal of Physical* Chemistry 36, no. 4 (2002): 1152-1155.

[7] C. Hodgman, D. Charles, *Handbook of Chemistry and Physics*, Chemical Rubber Publishing Co., 1951

[8] M. Buback, J. Schweer, and H. Tups. "Near Infrared Absorption of Pure Carbon Dioxide up to 3100 bar and 500 K. II. Wavenumber Range 5600 cm^{-1} to 7400 cm^{-1}," *Zeitschrift für Naturforschung A*, 41(3), pp. 512-518, Mar. 1986.

[9] I. Dicaire, J. C. Beugnot, and L. Thévenaz, "Analytical modeling of the gas-filling dynamics in photonic crystal fibers", *Applied optics*, 49(24), pp.4604-4609, Aug. 2010.

[10] N. D. Gupta, and S. K. Ghosh, "A report on the Wilson cloud chamber and its applications in physics," *Reviews of Modern Physics*, 18(2), p. 225, Apr. 1946.

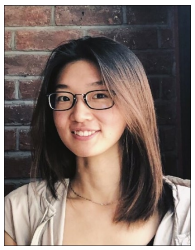

Yuting Yang received the B.Sc. degree in geophysics from the Peking University, Beijing, China, in 2017 and the M.Sc. degree in nuclear technology and applications from the Peking University, in 2020.

In 2021, she joined the Swiss Federal Institute of Technology of Lausanne (EPFL), Switzerland, as a Doctoral Research Assistant. Her main research interest is focused on distributed optical fiber sensing, especially based on Rayleigh scattering and Brillouin scattering.

Marcelo A. Soto received the PhD degree in Innovative Technologies of ICT Engineering, with a major in Optical Communications, from Scuola Superiore Sant'Anna, Italy, in 2011. During 2010–2011, he was a Research Fellow at Scuola Sant'Anna, where he worked on Raman and Brillouin distributed fiber sensors. Later, from 2011 to 2017, he was a Postdoctoral Researcher at the EPFL Swiss Federal Institute of Technology of Lausanne, Switzerland, where he worked on high-performance Brillouin and Rayleigh distributed sensing, nonlinear fiber optics, optical signal processing, and optical Nyquist pulse generation. In 2018, he joined Universidad Técnica Federico Santa María, Chile, where he is now an Associate Professor since 2022 and leads a research group on distributed fiber sensing. Between 2018 and 2021, he also had an invited position as one of the "100 distinguished invited professors" at Guangzhou University, China.

Dr. Soto is author or coauthor of over 220 publications in international journals and conferences, 3 book chapters and 9 patents in the fields of optical communications and optical fiber sensing. He has served as a Technical Committee Program Member of several major conferences in the field of optical fiber sensing. He has also been an Associate Editor of the Optical Fiber Technology Journal and the IEEE Journal of Lightwave Technology.

Dr. Soto is a Senior Member of Optica (former OSA), and Member of the Institute of Electrical and Electronics Engineers (IEEE).

Luc Thévenaz received the M.Sc. degree and the Ph.D. degree in physics from the University of Geneva, Switzerland. In 1988 he joined the Swiss Federal Institute of Technology of Lausanne (EPFL) where he is now Emeritus Professor and has led a research group active in photonics. Research topics include fiber sensors, slow & fast light, nonlinear fiber optics and laser spectroscopy in gases. His expertise covers all applications of stimulated Brillouin scattering in optical fibers and he is known for his innovative concepts related to distributed fiber sensing pushing beyond barriers.

During his career he stayed at Stanford University, at the Korea Advanced Institute of Science and Technology (KAIST), at Tel Aviv University, at the University of Sydney and at the Polytechnic University of Valencia. In 2000 he co-founded the company Omnisens that is developing and commercializing advanced photonic instrumentation based on distributed fiber sensing.

He was member of the Consortium in the FP7 European Project GOSPEL "Governing the speed of light", was Chairman of the European COST Action 299 "FIDES: Optical Fibres for New Challenges Facing the Information Society" and was Coordinator of the H2020 Marie Skłodowska-Curie Innovative Training Networks FINESSE (FIbre NErve Systems for Sensing). He is member of the Steering Committee of the International Conference on Optical Fiber Sensors and General Chairman of this conference in 2018. He has served in the Technical Committee of several conferences, such as ECOC, CLEO-Europe, APC, etc and has been Associate Editor of Photonics Technology Letters and the Journal of Lightwave Technology. He is now co-Executive Editor-in-Chief of the journal Nature Light: Science & Applications.

He is Fellow of the IEEE and Optica (OSA), and Member of the Swiss Academy of Engineering Sciences.